ORIGINAL ARTICLE

A pilot study on an electromagnetic tracking system using tunneling magnetoresistance (TMR) sensors applicable to a 4F catheter (1.4 mm in diameter)

Rina Nagano[1] · Kazuaki Hara[1] · Etsuko Kobayashi[1] · Takashi Ohya[2] · Ichiro Sakuma[1]

Abstract

Purpose Tracking the position and orientation of a 4F catheter (ϕ 1.4 mm) is required in superselective intra-arterial chemotherapy (SSIAC). Tunneling magnetoresistance (TMR) sensors, which measure magnetic fields, are promising candidates because the size of the TMR sensor can be less than a few tenths of a millimeter. The purpose of this paper is to prove the feasibility of an EMT system utilizing TMR sensors as magnetometers.

Methods Three 1-axis TMR sensors (0.3 mm × 0.3 mm) were packaged on a flexible printed circuit board (PCB) together with an amplifier chip. The PCB was integrated into a 4F catheter. Six field generator coils driven by alternating current (AC) at different frequencies were used. Magnetic field measurement errors were evaluated to assess the effect of electromotive force (EMF) on TMR-based sensing by changing the coils' driving frequencies. The tracking error was also evaluated. As a result, the feasibility of catheter navigation utilizing the EMT system was demonstrated.

Results There was a positive correlation between the frequency and the magnetic field measurement error using the TMR sensor ($R^2 = 0.999$). With magnetic field frequencies less than 603 Hz, the average position and orientation estimation error were 10.1 mm and 2.3 degree, respectively. Under ideal conditions, the average estimation error values were 0.9 mm and 0.3 degree, respectively.

Conclusion The position and orientation errors varied with frequency owing to the induced electromotive force. We should consider the effect of electromotive force on TMR sensor assemblies caused by alternating magnetic fields. An EMT system using TMR sensors was validated, although room for further improvement was identified.

Keywords Tunneling magnetoresistance effect · Magnetic sensor · Catheter navigation · Oral cancer

Introduction

Superselective intra-arterial chemoradiotherapy (SSIAC) is an effective way to treat oral cancer [1, 2]. In this treatment, a surgeon inserts a 4F catheter retrograde into the superficial temporal artery, guides it to the artery that feeds the tumor, and injects anticancer drugs directly through the catheter. This approach can apply anticancer drugs in higher concentrations compared to those in conventional chemotherapy.

Therefore, this treatment has been attracting attention in recent years.

The standard procedure of SSIAC is summarily described in [3]. (1) A guide-wire is inserted into the common carotid artery from the superficial temporal artery (STA). (2) A vinyl hook-shaped catheter is inserted into the STA along the guide-wire (outer diameter 4Fr (1.33 mm)). (3) The guide-wire is removed. Then, the catheter is drawn. (4) The tip of the catheter is inserted to the target artery by drawing it back under fluoroscopic guidance. A catheter navigation system is required to guide the vinyl hook-shaped catheter. Finally, several procedures are conducted to place the drug infusion catheter to the target artery. In step (4), the position and rotation of the tip of the hook-shaped catheter should be carefully controlled so that position and the bent tip direction are aligned with the entry hole of the distal target artery. When the hook-shaped catheter is appropriately positioned

✉ Ichiro Sakuma
  sakuma@bmpe.t.u-tokyo.ac.jp

1 Graduate School of Engineering, The University of Tokyo, Tokyo, Japan

2 Graduate School of Medicine, Yokohama City University, Yokohama, Japan

and aligned, its tip autonomously enters the distal target artery because of its elastic properties. Catheter navigation system utilizing EMT is expected to reduce the difficulties in positioning and aligning the catheter. In this procedure, currently available EM tracking system with miniaturized sensor does not provide rotation angle around the catheter axis.

In this therapeutic procedure, a surgeon must track the position and orientation of the catheter tip to manipulate the catheter so that it is inserted into the target branch. Currently, intraoperative X-ray fluoroscopy is used to track the catheter tip. However, it is often difficult to identify the orientation and position of the catheter, leading to increased radiation exposure, both to surgeons and patients, and an increase in the use of contrast agents. Therefore, the catheter tip must be tracked to navigate this surgical intervention in the above-mentioned step (4). Intraoperative ultrasound is an alternative way to track the catheter. However, it is still challenging to visualize target branches with small diameters using conventional ultrasound imaging technologies. Catheter navigation based on conventional technologies in computer-aided surgery utilizing a miniaturized electromagnetic tracking (EMT) system is another possible solution.

EMT is widely used to track surgical devices in the body [4–7]. Currently available 5-D EM tracking system with miniaturized sensor does not provide rotation angle around the catheter axis. It is possible to use the two 5D sensors installed both at the tip and a proximal location of a catheter and proximal to verify the bending of a hook-shaped catheter [8]. We have already considered this concept in our previous study [9]. The diameters of the currently available 5D EMT sensors are sufficiently small (0.3–0.92 mm in diameter [10]) and their lengths are longer than 5.5 mm. Stock et al. reported that the diameter of SAT is 2.03 ± 0.33 mm in cadaveric studies [11]. Piazza et al. reported the effect of bending sensors on precision of coil-based EMT with 3-mm bending radius [12] although the precision of the EMT under bending up to 6-degrees showed good precision up to 40 degrees bending. They observed broken sensors in 50 degrees of bending. Considering the diameter of STA, it is not appropriate to apply currently available 5-D EM tracking system to catheter navigation for SSIAC. The dimensions of some commercially available EMT sensors providing 6 degrees of freedom (3 axes of translation and 3 axes of rotation) are (ϕ 0.92 mm in diameter $\times$ 9.4 mm in length) [10], (ϕ 0.56 mm $\times$ 12 mm in length), and (ϕ 0.9 mm $\times$ 7.25 mm length) [13]. In SSIAC for oral cancer, the 4F guiding catheter (ϕ 1.3 mm in diameter) is commonly used. However, a conventional EMT system cannot be applied to SSIAC because the length of the magnetic sensor is too long (> 7.25 mm) to be integrated at the 4F catheter tip (ϕ 1.3 mm) with sufficient flexibility. For application to SSIAC, radius of curvature of a catheter is required as small as a few mm to follow the target vascular branch.

Tunneling magnetoresistance (TMR) sensors, which measure magnetic fields based on the tunneling magnetoresistance effect, are promising candidates, as the size of the TMR can be less than a few tenths of a millimeter. When constructing an EMT system incorporating miniaturized multiple magnetometers, multiple external alternating magnetic fields with different frequencies are usually used to encode information about distances between the magnetometer and magnetic field generator coils [14]. Dai et al. reported the use of commercially available tri-axial magneto-resistive sensor to 6-D electromagnetic tracking [15]. However, the size of their sensor system is too large to be installed in a catheter. A typical TMR sensor has three main layers, from bottom to top: a pinned ferromagnetic layer, a tunnel barrier layer, and a free ferromagnetic layer, forming a magnetic tunnel junction element [16]. The sensor chip is also packaged on a printed circuit board (PCB). Under this implementation, the AC magnetic fields create an induced electromotive force on the substrate of the TMR sensors or PCB, which may cause errors in the TMR sensor measurement. Electromotive force generated in the circuit loop on the sensor unit assembly is proportional to time derivative of the magnetic flux density originated from field generator coil. Although this component is efficiently removed by synchronous detection with the drive current waveform, there are remaining components due to synchronous detection characteristics and the phase characteristics of the circuit loop. In case of coil-based measurement for EMT, signal intensity increases as the frequency of the driving current for the field generator increases even though the magnitude of noise increases. As a result, signal-to-noise ratio does not deteriorate. On the other hand, magnitude of signal does not change with the increase in the driving current for the field generator because the TMR sensor measures the magnetic field intensity itself, not time derivative of magnetic flux density. It is considered that the noise level is subject to electromotive force generated on the TMR sensor circuit unit.

The purpose of this paper is to prove the feasibility of an EMT system utilizing TMR sensors as magnetometers. We fabricated an 4F catheter with three integrated TMR sensors. Then, we constructed a prototype of a TMR-based EMT system and developed tracking algorithm. The accuracy of the developed EMT system, the influence of the induced electromotive force on magnetic field measurement, and the resultant position and posture estimation accuracy were evaluated. Finally, the feasibility of catheter navigation utilizing the EMT system was demonstrated by visualizing the location of the catheter in a navigation display.

Methods

Catheter (4F, 1.4 mm) with three integrated TMR sensors

Three 1-axis TMR sensors were mounted orthogonally on a catheter. Each TMR sensor measured the magnetic field in the sensor sensitivity direction by aligning the sensors depending on the pinned ferromagnetic layer of each TMR. A constant voltage source (5.0 V) was applied to the TMR sensors and a fixed resistor connected in series. The voltage divided between two TMR terminals was fed into an onboard amplifier. The manufactured 4F catheter is shown in Fig. 1. Three sensors were packaged on a flexible printed circuit board (PCB) together with an amplifier chip, as shown in Fig. 1a. The sensor units were custom-made for this project by Daido Steel Co., Ltd. The manufacturer of the sensor units integrated custom-made TMR sensor elements on a small PCB board together with an amplifier and resister. The manufacturer conducted calibration to quantify the relationship between sensor unit output and external magnetic field under their calibrated experimental environment. The relation between the external magnetic field and output voltage was evaluated before integrating the system into the catheter. The calibration data were provided to the authors. We used the same driving condition as the calibration process and referred to the data sheet of each sensor unit. Three slits were fabricated in the cylindrical tube. The TMR sensor, reference

TMR without magnetization for temperature compensation, resister, and amplifier were integrated on PCB as shown in Fig. 1a. Then, the tip side of the catheter was closed with polymers. We did not make a hook-shaped catheter. In this pilot study, we put the sensor with a distance of 23 mm from the tip of the catheter.

Prototype EMT system

The field generator used in this system consisted of six coils positioned in an L shape, as shown in Fig. 2. Each coil was wound with 6060 turns of 0.5-mm-diameter enameled wire and had an outer diameter of 100 mm and a height of 100 mm. Each coil was driven by a constant current source with amplitude ranging from 1.58 to 2.04 A and from 302 to 1062 Hz, respectively. Details of the driving condition are shown in the following experimental section. The sensor output signals were fed to a 16-bit data acquisition system (USB-6229, National Instruments, USA) with input voltages ranging from 3.3 V to 4.0 V and a sampling frequency of 25,000 Hz. The sensor output voltage varied from 3.5 V to 3.8 V under the magnetic field, which varied from -33 to 33 A/m (-4.1 Oe to 4.1 Oe). The measurement range of the ADC was adjusted to monitor this voltage range to improve resolution in signal amplitude measurements. The experimental conditions are described in 2.6.

Fig. 1 Catheter (4F, 1.4 mm) with three integrated TMR sensors. **a** Integration of the three TMR sensors in the catheter, **b** External view of the catheter **c** The PCB with the three TMR sensors was integrated at approximately 23 mm from the tip of the catheter
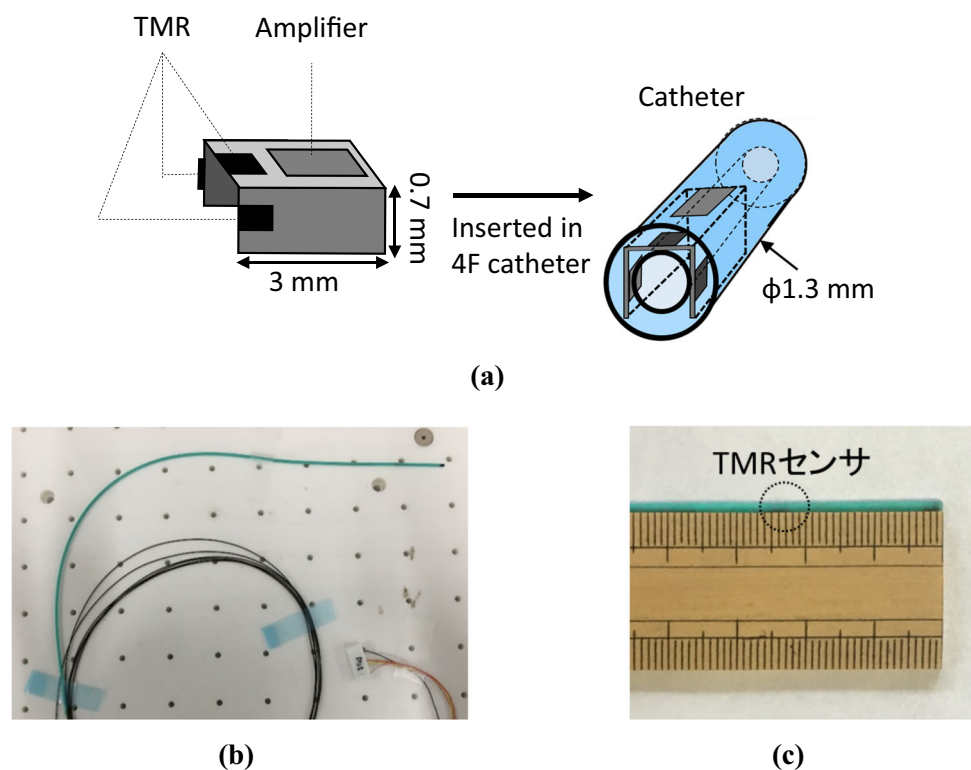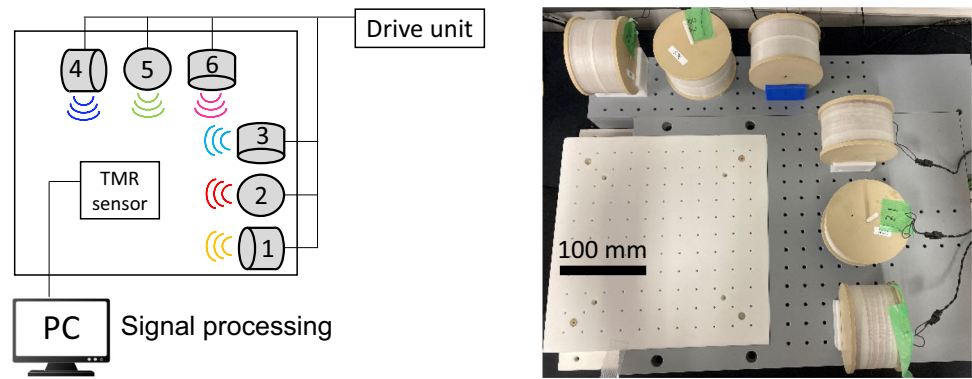
Fig. 2 Experimental setup

Experimental setup

To measure the sensor signals at known positions from six field generator coils, the experimental system shown in Fig. 2 is prepared. The six field-generating coils were positioned by inserting pins (ϕ 2.5 mm) fixed to the coil holder. The catheter with the integrated sensor unit was fixed in a sensor holding jig that was positioned by pins inserted into holes machined at 25.0 mm intervals. The precision of translational and rotational positioning was 0.3 mm and 1.5 degree, respectively. The holes on the plate shown in Fig. 2 and holes attached to the jig were fabricated with tolerances to achieve these precisions. To avoid magnetic interference, the base plate was made of polyvinyl chloride, and the coil holders and sensor holding jig were made of polyoxymethylene.

The measurement volume was set as 500 × 600 × 300 mm, considering the anatomical region of interest of SSIAC. The six coils were positioned as shown in Fig. 2. The coil positions and sensor holder position were controlled by inserting pins with the holders into the holes on the base plate.

Three sensor elements were integrated in the catheter as shown in Fig. 1a. The position of the catheter was defined as the position of the sensing unit determined by the jig. The position data were represented as relative position referring to the plate.

Tracking algorithm

We developed a tracking algorithm to estimate the sensor position $\boldsymbol{P}(x, y, z)$ and orientation $\boldsymbol{R}(\theta, \phi, \psi)$ from the TMR sensor output voltage $\boldsymbol{V}_m$ shown in Fig. 3. The algorithm searches for $\boldsymbol{P}$, $\boldsymbol{R}$ so that the theoretical sensor output voltage $\boldsymbol{V}_t(\boldsymbol{P}, \boldsymbol{R})$ calculated from the assumed $\boldsymbol{P}$, $\boldsymbol{R}$ converges to the measured sensor output voltage $\boldsymbol{V}_m$ using the Levenberg–Marquardt algorithm. The theoretical sensor output voltage is calculated using the theoretical magnetic field value $\boldsymbol{H}_t(\boldsymbol{P})$. $\boldsymbol{P}$, $\boldsymbol{R}$ is repeatedly updated until the residual position error $\Delta\boldsymbol{P}$ becomes less than 0.1 mm.

Calculation of magnetic field

The theoretical sensor outputs are calculated based on the theoretical magnetic field value corresponding to assumed position of the TMR sensor. The theoretical magnetic field is calculated by modeling a coil as a superposition of circular current as shown in Fig. 4. Based on the Biot–Savart law, a single circular current creates the magnetic field vector potential $\overrightarrow{H}(H_r, H_\theta, H_z)$ at $P(r, \theta, z)$ as determined by (1)–(3), where r, θ, z are coordinates in a polar cylindrical coordinate system.

$$H_r(r, \theta, z)$$
$$= -\frac{Ikz}{4\pi\sqrt{ar^3}}\left(\int_0^{\frac{\pi}{2}} \frac{d\phi}{\sqrt{1 - k^2\sin^2\phi}} - \frac{2 - k^2}{2(1 - k^2)}E(k)\right) \tag{1}$$

$$H_\theta(r, \theta, z) = 0 \tag{2}$$

$$H_z(r, \theta, z)$$
$$= \frac{Ik}{4\pi\sqrt{ar^3}}\left(\int_0^{\frac{\pi}{2}} \frac{d\phi}{\sqrt{1 - k^2\sin^2\phi}} + \frac{k^2(a + r) - 2r}{2(1 - k^2)}E(k)\right) \tag{3}$$

where a : radius of coil r, θ, z are coordinates in a polar cylindrical coordinate system

$$k = \sqrt{\frac{4ar}{(r + a)^2 + z^2}}$$

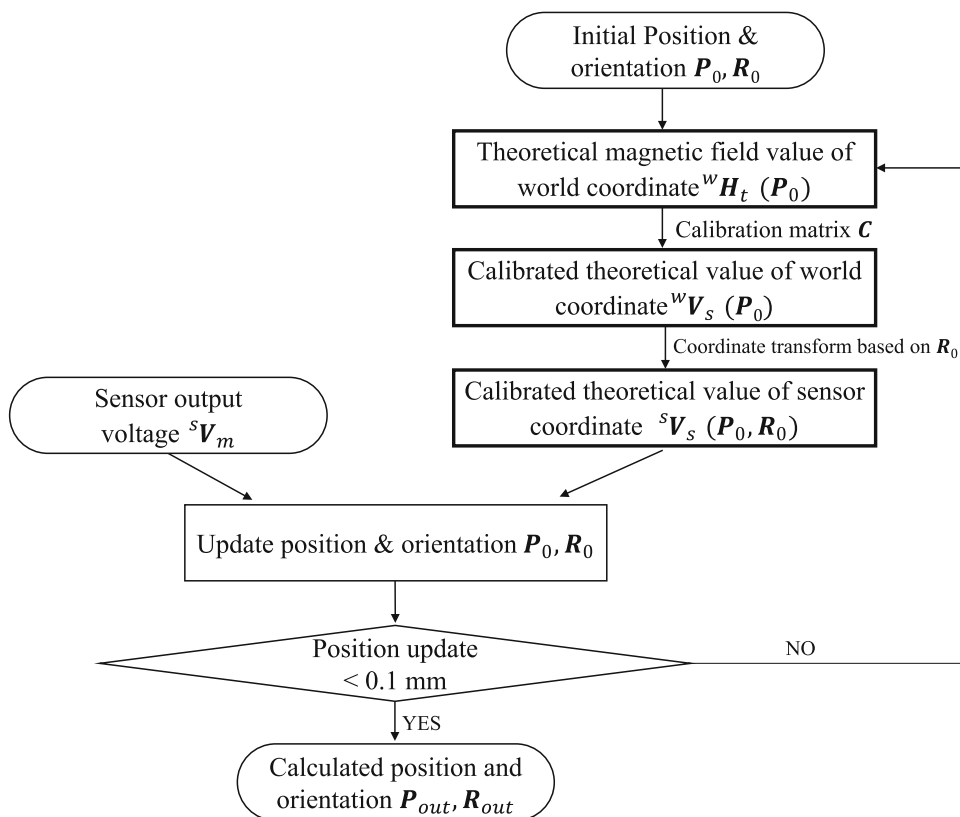$$\boldsymbol{\theta} - \boldsymbol{\varphi} = 2\boldsymbol{\phi} - \boldsymbol{\pi}$$

$$E(k) = \int_0^{\frac{\pi}{2}} \sqrt{1 - k^2\sin^2\phi}\, d\phi$$

(Complete elliptic integral of the second kind)

The magnetic field at a sensor position from each coil with N number of turns is calculated as the sum of a circular current using (4).

Fig. 3 Tracking algorithm of TMR sensor-based electromagnetic tracking system

$$H = \sum_{k=1}^{N} H(r_k, \theta_k, z_k) \tag{4}$$

Finally, the theoretical magnetic field from each coil is obtained as an 18-dimensional vector data.

$$\begin{bmatrix} H_{t\_1x} & H_{t\_1y} & H_{t\_1z} & H_{t\_2x} & \cdots & H_{t\_6z} \end{bmatrix}$$

The theoretical magnetic field is calculated by modeling a coil as a superposition of circular current.

Calibration of sensor output

The magnetic fields are calculated as an 18-dimensional vector consisting of three-dimensional magnetic fields generated from six coils. To consider the effect of coil winding inhomogeneity, mutual inductance between the coils, and TMR sensor setting errors, the following calibration process was introduced. The theoretical 18-dimensional magnetic field vector is converted to the simulated value of sensor outputs voltage using the calibration matrix C. The calibration matrix C is predefined by measuring the sensor outputs voltage at n known test points and comparing them with the theoretical magnetic field value at test points beforehand. Thus, C was determined through the calibration process.
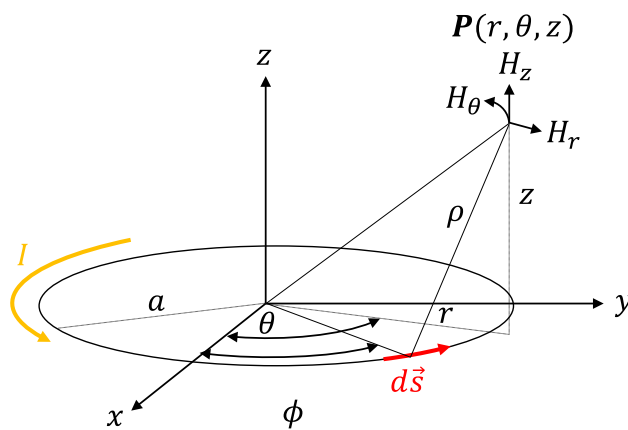

Fig. 4 Modeling the magnetic field induced by a coil

Since the calculated output voltage corresponds to the calculated magnetic field, the voltage is also an 18-dimensional vector. The matrix is defined by the following equation.

$$C = \begin{bmatrix} c_{11} & c_{12} & & c_{1,19} \\ c_{21} & c_{22} & & c_{2,19} \\ c_{31} & c_{32} & & c_{3,19} \\ & & \ddots & \vdots \\ c_{18,1} & c_{18,2} & \cdots & c_{18,19} \end{bmatrix} \tag{5}$$

Because $\boldsymbol{H}_t$ is a collection of magnetic field vectors due to each of the six coils at calibration points $P_1 \cdots P_n$, we can define $\boldsymbol{H}_t$ to consider the translational and rotational error of TMR sensor positioning.

$$
\boldsymbol{H}_t = \begin{bmatrix}
H_{1x}(P_0) & H_{1x}(P_1) & \cdots & H_{1x}(P_n) \\
H_{1y}(P_0) & H_{1y}(P_1) & & H_{1y}(P_n) \\
H_{1z}(P_0) & H_{1z}(P_1) & & H_{1z}(P_n) \\
H_{2x}(P_0) & H_{2x}(P_1) & & H_{2x}(P_n) \\
H_{2y}(P_0) & H_{2y}(P_1) & & H_{2y}(P_n) \\
H_{2z}(P_0) & H_{2z}(P_1) & & H_{2z}(P_n) \\
\vdots & \vdots & \ddots & \vdots \\
H_{6z}(P_0) & H_{6z}(P_1) & \cdots & H_{6z}(P_n) \\
1 & 1 & & 1
\end{bmatrix} \quad (6)
$$

If we set the measurement of voltage signals of three sensors at position $P_1 \cdots P_n$,

$$
\boldsymbol{V}_m = \begin{bmatrix}
V_{1x}(P_0) & V_{1x}(P_1) & \cdots & V_{1x}(P_n) \\
V_{1y}(P_0) & V_{1y}(P_1) & & V_{1y}(P_n) \\
V_{1z}(P_0) & V_{1z}(P_1) & & V_{1z}(P_n) \\
V_{2x}(P_0) & V_{2x}(P_1) & & V_{2x}(P_n) \\
V_{2y}(P_0) & V_{2y}(P_1) & & V_{2y}(P_n) \\
V_{2z}(P_0) & V_{2z}(P_1) & & V_{2z}(P_n) \\
\vdots & \vdots & \ddots & \vdots \\
V_{6z}(P_0) & V_{6z}(P_1) & \cdots & V_{6z}(P_n)
\end{bmatrix} \quad (7)
$$

then the calibration matrix C is determined through least squares estimation as follows:

$$
\boldsymbol{H}_t \boldsymbol{C} = \boldsymbol{V}_m \quad (8)
$$

$$
\boldsymbol{C} = \left(\boldsymbol{H}_t^T \boldsymbol{H}_t \right)^{-1} \boldsymbol{H}_t^T \boldsymbol{V}_m \quad (9)
$$

Experimental

Influence of induced electromotive force evaluation

To determine the effect of electromotive force on the sensor outputs, we rotated the catheter, which was placed parallel to the X-axis of the experimental table by 180 degrees about the catheter axis, and compared the sensor output signals. These postures are defined as postures A and B, respectively. Posture A was the same posture as that used in the calibration, and posture B was that where the catheter was rotated by 180 degrees relative to the posture A. The magnetic field intensity is the same in opposite direction under this condition. However, if the electromotive force exerts an

influence, there should be differences in the signal amplitudes. We also checked the dependency of these differences on magnetic field frequencies at 435, 532, and 1062 Hz with a current of 0.18 A. To evaluate the measurement errors, the TMR sensor-mounted catheter was placed at 135 points in a 100 mm × 200 mm × 100 mm space with the two postures rotated 180 degree about the catheter axis. The catheter was fixed using positioning pins with a positioning accuracy of 0.3 mm and 1.5 degree.

The error of the magnetic field measurement ΔV due to the posture is determined using Eq. (10). $V_k(R)$ represents the output voltage of k-axis TMR sensors with posture R.

$$
\begin{aligned}
&\Delta V \\
&= \sqrt{(|V_x(A)| - |V_x(B)|)^2 + (|V_y(A)| - |V_y(B)|)^2 + (|V_z(A)| - |V_z(B)|)^2}
\end{aligned} \quad (10)
$$

Sensor calibration and position tracking accuracy evaluation

The six coils for magnetic field generation had the same parameters as in the first experiment and were driven at 302, 345, 395, 435, 532, and 602 Hz. To form the calibration matrix, the TMR sensor-mounted catheter was placed at 68 points, shown as green squares in Fig. 5, and the sensor output voltages with posture A were measured. To evaluate the position and orientation accuracy, the catheter was placed at 67 points, shown as red triangle triangles in Fig. 5, with postures A and B. The estimation errors under the same posture as that used in the calibration process (posture A) and those with a different posture (posture B: 180 degrees rotated about the catheter axis) were measured. The experimental conditions are summarized in Table 1.

The position error e_p between the real position (x_r, y_r, z_r) and the calculated position (x_c, y_c, z_c) is determined using (11).

$$
e_p = \sqrt{(x_c - x_r)^2 + (y_c - y_r)^2 + (z_c - z_r)^2} \quad (11)
$$

The orientation error e_o between the real orientation $(\theta_r, \phi_r, \psi_r)$ and the calculated orientation $(\theta_c, \phi_c, \psi_c)$ is determined using (12).

$$
e_o = \frac{|\theta_c - \theta_r| + |\phi_c - \phi_r| + |\psi_c - \psi_r|}{3} \quad (12)
$$

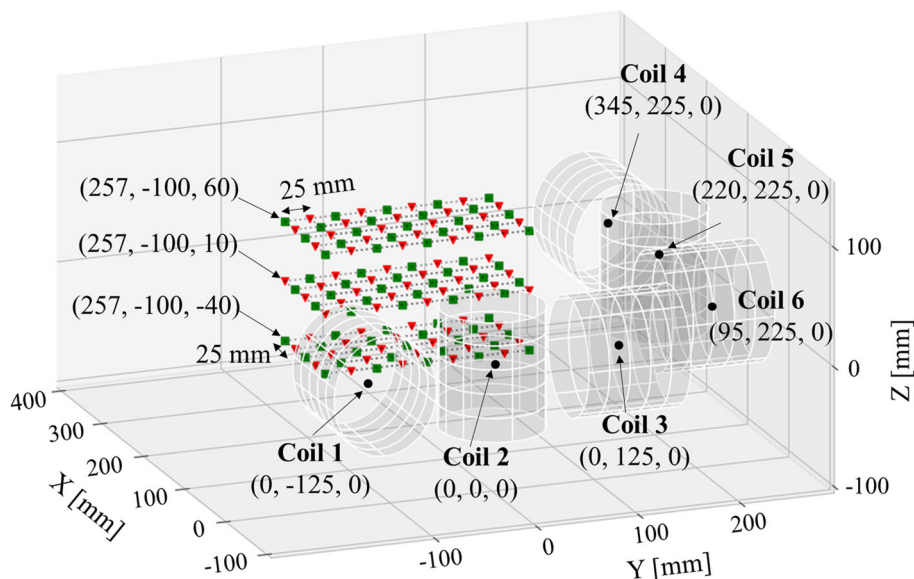**Fig. 5** Experimental setup to evaluate EMT system using TMR sensors

Table 1 Experimental conditions of the experiment

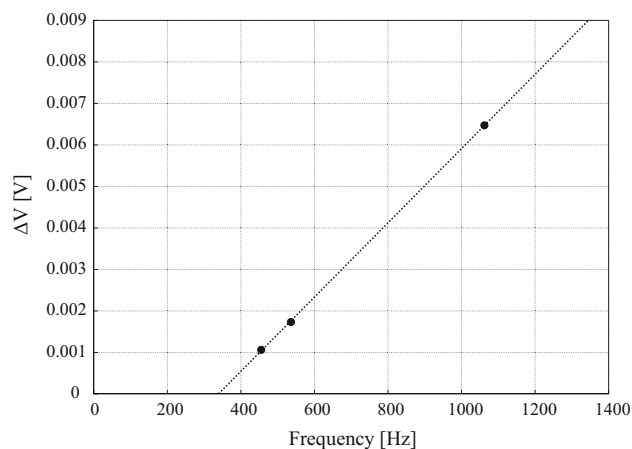| Coil parameter	Diameter (mm)	100
	Height (mm)	55
	Number of turns (−)	6060
	Winding diameter (mm)	0.5
Drive frequency of the coil (Hz)		345, 435, 602, 734, 881, 1062
Current flowing through the coil (A)		0.19, 0.16, 0.18, 0.17, 0.20, 0.17
Measurement time (ms)		200
Measurement sampling frequency (Hz)		25,000

Fig. 6 The relationship between frequency and ΔV

Results

Magnetic field measurement error due to sensor posture

As shown in Fig. 6, there was a positive correlation between frequency and the error of the magnetic field measurement ΔV due to the posture (A) and (B).

This result suggests that the induced electromotive force does affect the sensor output.

Position and orientation errors

For posture A, the average position error e_p of 135 points was 0.9 mm, while the average orientation error e_o of 135

points was 0.3 degree. For posture B, e_p was 10.1 mm, while e_o was 2.4 degree. The results are shown in Fig. 7.

When the posture of the sensor was identical to that used in calibration, the estimation performance was sufficient for use as an EMT system. On the contrary, as shown in 3.1, there were magnetic field measurement errors due to posture of the TMR sensor. These errors affect the system's EMT performance.

In Table 2, position and orientation errors are summarized. Error for each axis is presented.
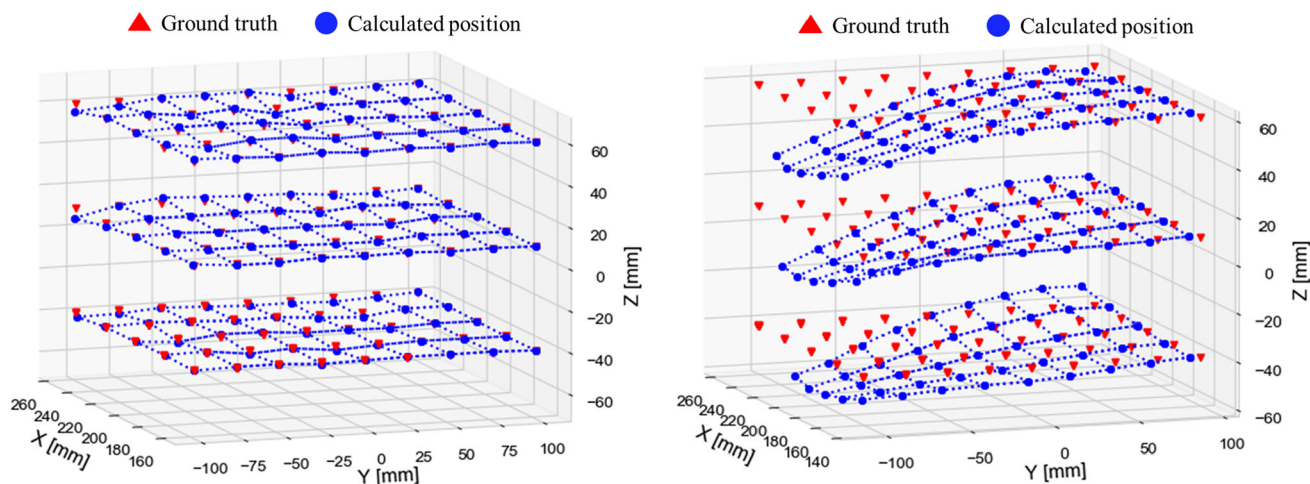
Fig. 7 Position and orientation error. Red points stand for the grand truth data based on the catheter holding jig's position. Blue dots stand for the estimated position. Measurement points are not identical to the measurement points used in calibration process

Table 2 Position and orientation errors

Condition		e_p (mm)				e_o (degree)		
		Mean	Max.	Min.		Mean	Max.	Min.
A	All	0.9	4.8	0.0	All	0.3	1.2	0.0
	Δx	-0.1	0.6	-0.9	$|\Delta\theta|$	0.3	1.6	0.0
	Δy	0.0	1.2	-1.4	$|\Delta\varnothing|$	0.2	2.0	0.0
	Δz	-0.1	2.3	-4.6	$|\Delta\psi|$	0.1	0.7	0.0
B	All	10.1	44.5	0.7	All	2.4	8.3	0.0
	Δx	2.8	-8.7	13.4	$|\Delta\theta|$	2.3	7.7	0.0
	Δy	-2.4	-24.2	5.9	$|\Delta\varnothing|$	3.5	14.9	0.3
	Δz	-3.8	-41.0	8.3	$|\Delta\psi|$	1.3	3.5	0.0

Discussion

Contribution of the present work

To realize catheter navigation system for SSAIC, a miniaturized 6D EMT system should be developed. This study showed the feasibility of a EMT system using tunneling magnetoresistance (TMR) sensors applicable to a 4F catheter. TMR measures intensity of magnetic field, whereas conventional coil-based tracking sensors measures time derivative of flux density of the magnetic field. This study reveals that this difference in principle of measurement of magnetic field brings about large effect of electromotive force generated in electric circuit in the sensor assembly on measurement performance. Although further validation and improvement of the system are required, it is considered that we can realize a 6D EMT for thin catheter that is not possible using currently available EMT systems.

Influence of induced electromotive force

ΔV, the magnetic field error due to the posture, tends to increase as the external magnetic field frequency increases. This is thought to be a result of the induced electromotive force on the sensor substrate.

Based on the size of the TMR sensor substrate (0.7 mm × 3 mm), the theoretically induced electromotive force (EMF) on the substrate was calculated to be 2.2×10^{-6} V, which was different from the observed ΔV. This is because of the soft magnetic yoke or ferromagnetic layer contained in TMR sensors and the operational amplifier. The soft magnetic yoke is mainly composed of iron and has high permeability. Because the permeability of iron is more than 1000 times greater than the permeability of a vacuum, the real induced electromotive force may be greater than the theoretical value. Furthermore, the sensor output voltage was amplified by an operational amplifier. The amplification factor of the operational amplifier is unknown because it has not been provided by the
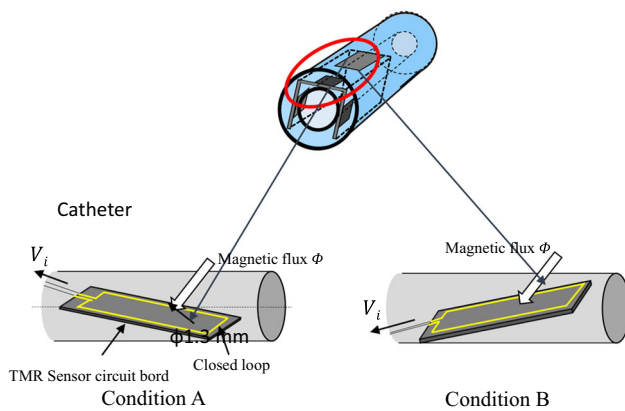
Fig. 8 Effect of errors of sensor assembly mounting on EMF. The magnitude of magnetic flux causes EMF changes in the case of 180-degree rotation about the catheter axis when the sensor assembly is mounted at a slight incline

manufacturer, but this can explain the difference between the theoretically induced EMF and the observed values.

Other factors affecting the magnetic field measurement error, ΔV, are small changes in the position of the sensor inside the catheter due to posture and errors in the mounting angle of the sensor. For a conventional EMT system incorporating miniaturized pickup coils, these errors in posture during fabrication can be compensated by using an appropriate calibration method similar to our tracking algorithm. However, this type of error cannot be removed. The magnitude of magnetic flux causing EMF and that when the catheter is rotated by 180-degree about the catheter axis are not the same when sensor assembly is mounted slightly inclined as shown in Fig. 8.

The TMR sensor units are mounted off the central axis of the catheter; therefore, when the sensor is rotated about the axis, there is a maximum displacement of 1.4 mm in the worst case, which is the diameter of the catheter. However, magnetic field intensities estimated by theoretical calculation at 1.4 mm separated positions could not explain the ΔV we observed. There may be an error in the mounting angle, which is another factor contributing to ΔV.

Changes in the mounting position can also cause magnetic field measurement errors, although they are independent of the frequency. The effect of driving frequencies on resultant position and orientation errors should be investigated in future study.

In the conventional EMT method utilizing small pickup coils, the EMF itself constitutes the signals to be measured for estimating the magnetic field intensity. However, in case of TMR-based magnetometer sensing, the TMR sensor directly measures the magnetic field intensity as an alternating magnetic field. The effect of electromotive force on the resultant signal is complex; it may affect the TMR sensor itself in

addition to the pickup electric circuit. Hysteresis in magnetoresistance to an external magnetic field has also been reported [16, 17]. A detailed analysis of phase information in the measured signal relative to the driving signals of the magnetic field generator coils should be performed to clarify the mechanism of error generation. As an alternative approach, the packaging design of the PCB of the magnetic sensors can be optimized. We can also reduce the frequency of coil driving current. However, this may reduce the sampling frequency of the EMT system.

When hysteresis exists, signal from TMR sensor is distorted because the sensor output to upstroke of intensity of the magnetic field generated by the field generator coil differs from that in the down stroke, this signal may cause errors in magnetic fiels intensity measurements. Further investigation should be conducted to clarify if hysteresis is one of the causes of tracking errors. The effect of driving frequencies on resultant position and orientation errors should be investigated in future study.

Position and orientation accuracy

We studied the feasibility of small TMR sensors in EMT for catheter tracking. We could sufficiently reduce the size of the tracking sensor element integrated in a 4F catheter (1.4 mm in diameter). Miniaturization of the tracking sensor element leads to better flexibility of the catheter, enabling a smaller radius of curvature. We assumed the required accuracy for catheter tracking in SSIAC is 1 mm and 15 degree considering diameter of target arteries and STA as large as a few mm. The position accuracy ($e_p = 10.1$ mm) was not sufficient for SSIAC, while the orientation accuracy ($e_o = 2.3$ mm) in posture A was sufficient. However, in the condition in which measurement errors do not affect the results (posture A), the position and orientation accuracy ($e_p = 0.9$ mm, $e_o = 0.4$ mm) meet the requirements for SSIAC. This result indicates that the proposed EMT system using TMR sensors is promising for catheter tracking in small and complex vasculature networks, such as those involved in SSIAC.

We focused on the rotation around the catheter. The rotation around axis is the most important orientation information in SSIAC since it determines a hook-shaped catheter tip's orientation in the STA relative to the orientation of entrance of distal target artery. We evaluated the basic orientation (A) or the rotation by 180 degrees (B) since the purpose of the present study is to establish the proof of concept of an electromagnetic tracking system using tunneling magnetoresistance (TMR) sensors applicable to a 4F catheter. More detailed evaluation for different orientation as shown in [18] should be conducted to validate the proposed system.

The position and orientation errors were determined by the sensor output voltage errors between the theoretical and

measured values and the Jacobian of the position and orientation calculation algorithm. The Jacobian is determined by the coil arrangement and current. The spatial gradient of the magnetic field should be designed to be as large as possible in the region of interest in the measurement volume. The present experimental coil arrangement is not yet optimized from this viewpoint. To increase the spatial gradient, the driving current of the coil can be increased as long as the magnetic field strength generated by the coil does not exceed the dynamic range of the TMR sensor, as in the case of conventional EMT systems.

Feasibility of Position and orientation accuracy

A blood vessel model (inner diameter: 2.5 mm, outer diameter: 4.5 mm) was placed in a human head phantom. Phantom was 3D printed based on a CT artificial data generated by a medical doctor who is one of the authors. The catheter navigation system was developed using open-source software Slicer [19]. The catheter navigation procedure was demonstrated to confirm the feasibility of catheter navigation utilizing the EMT system. A video clip showing a demonstration of catheter navigation is provided as supplementary information. The movement of the catheter tip in the blood vessel model was successfully visualized on the navigation display.

Conclusion

This paper proposed a new electromagnetic tracking system using TMR sensors that can be applied to superselective intra-arterial chemoradiotherapy (SSIAC). This system uses a miniaturized tracking element to reduce the catheter's minimum radius of curvature. Results of system evaluation experiments revealed that the position and orientation errors varied with frequency owing to the induced electromotive force. Unlike the case of a pickup coil-based magnetometer, we should consider the effect of electromotive force on the TMR sensor assembly caused by an alternating magnetic field. The prototype TMR-based EMT system achieved a position error of 0.9 mm and an orientation error of 2.3 degree where the field-generating coils and sensor holding jig were the same as the calibration process. Although the system has room for further validation and improvement, this EMT system using TMR sensors is promising for catheter navigation in SSIAC.

Declarations

References

1. Tohnai I, Fuwa N, Hayashi Y, Kaneko R, Tomaru Y, Hibino Y, Ueda M (1998) New superselective intra-arterial infusion via superficial temporal artery for cancer of the tongue and tumour tissue platinum concentration after carboplatin (CBDCA) infusion. Oral Oncol 34:387–390. https://doi.org/10.1016/S1368-8375(98)00018-9
2. Kobayashi W, Teh BG, Sakaki H, Sato H, Kimura H, Kakehata S, Nagahata M (2010) Superselective intra-arterial chemoradiotherapy with docetaxel–nedaplatin for advanced oral cancer. Oral Oncol 46(12):860–863. https://doi.org/10.1016/j.oraloncology.2010.10.001
3. Fuwa N, Kodaira T, Furutani K, Tachibana H, Nakamura T (2008) A new method of selective intra-arterial infusion therapy via the superficial temporal artery for head and neck cancer. Oral Surg, Oral Med, Oral Pathol, Oral Radiol Endodontol 105(6):783–789. https://doi.org/10.1016/j.tripleo.2007.07.031
4. Franz AM, Haidegger T, Birkfellner W, Cleary K, Peters TM, Maier-Hein L (2014) Electromagnetic tracking in medicine—a review of technology, validation, and applications. IEEE Trans Med Imag 33(8):1702–1725. https://doi.org/10.1109/TMI.2014.2321777
5. Friedman PA (2002) Novel mapping techniques for cardiac electrophysiology. Heart 87(6):575–582. https://doi.org/10.1136/heart.87.6.575
6. Wood B, Zhang H, Durrani A, Glossop N, Ranjan S, Lindisch D, Levy E, Banovac F, Borgert J, Krueger S (2005) Navigation with electromagnetic tracking for interventional radiology procedures: a feasibility study. J Vasc Interv Radiol 16(4):493–505. https://doi.org/10.1097/01.RVI.0000148827.62296.B4
7. Krücker J, Xu S, Glossop N, Viswanathan A, Borgert J, Schulz H, Wood BJ (2007) Electromagnetic tracking for thermal ablation and biopsy guidance: clinical evaluation of spatial accuracy. J Vasc Interv Radiol 18(9):1141–1150. https://doi.org/10.1016/j.jvir.2007.06.014
8. Condino S, Ferrari V, Freschi C, Alberti A, Berchiolli R, Mosca F, Ferrari M (2012) Electromagnetic navigation platform for endovascular surgery: how to develop sensorized catheters and guidewires. Int J Med Robot Comp Assist Surg 8(3):300–310. https://doi.org/10.1002/rcs.1417
9. Wang J, Ohya T, Liao H, Sakuma I, Wang T, Tohnai I, Iwai T (2011) Intravascular catheter navigation using path planning and

virtual visual feedback for oral cancer treatment. Int J Med Robot Comp Assist Surg 7:214–224. https://doi.org/10.1002/rcs.392

10. Aurora 5DOF Sensors (2022) https://www.ndigital.com/electromagnetic-tracking-technology/aurora/aurora-sensors/

11. Stock AL, Collins HP, Davidson TM (1980) Anatomy of the superficial temporal artery. Head Neck Surg 2(6):466–469. https://doi.org/10.1002/hed.2890020604

12. Piazza R, Nisar H, Moore J, Condino S, Ferrari M, Ferrari V, Peters TM, Chen EC (2020) Towards electromagnetic tracking of J-tip guidewire: precision assessment of sensors during bending tests. Med Imag: Image-Guided Proced, Robot Intervent Model, SPIE 11315:37–46. https://doi.org/10.1117/12.2549764

13. 3D Guidance 6DOF Sensors (2022) https://www.ndigital.com/electromagnetic-tracking-technology/3d-guidance/3d-guidance-sensors/

14. Jaeger HA, Franz AM, O'Donoghue K, Seitel A, Trauzettel F, Maier-Hein L, Cantillon-Murphy P (2017) Anser EMT: the first open-source electromagnetic tracking platform for image-guided interventions. Int J Comput Assist Radiol Surg 12(6):1059–1067. https://doi.org/10.1007/s11548-017-1568-7

15. Dai H, Song S, Zeng X, Su S, Lin M, Meng MQ-H (2017) 6-D electromagnetic tracking approach using uniaxial transmitting coil and tri-axial magneto-resistive sensor. IEEE Sens J 18(3):1178–1186. https://doi.org/10.1109/JSEN.2017.2779560

16. Hadjigeorgiou N, Asimakopoulos K, Papafotis K, Sotiriadis PP (2020) Vector: Magnetic field sensors: operating principles, calibration, and applications. IEEE Sens J 21(11):12531–12544. https://doi.org/10.1109/JSEN.2020.3045660

17. Miyazaki T, Tezuka N (1995) Giant magnetic tunneling effect in Fe/Al$_2$O$_3$/Fe junction. J Magn Magn Mater 139(3):L231–L234. https://doi.org/10.1016/0304-8853(95)90001-2

18. Hummel JB, Bax MR, Figl ML, Kang Y, Maurer C Jr, Birkfellner WW, Bergmann H, Shahidi R (2005) Design and application of an assessment protocol for electromagnetic tracking systems. Med Phys 32(7Part1):2371–2379. https://doi.org/10.1118/1.1944327

19. Fedorov A, Beichel R, Kalpathy-Cramer J, Finet J, Fillion-Robin J-C, Pujol S, Bauer C, Jennings D, Fennessy F, Sonka M (2012) 3D Slicer as an image computing platform for the quantitative imaging network. Magn Reson Imag 30(9):1323–1341. https://doi.org/10.1016/j.mri.2012.05.001